Proc. Natl. Acad. Sci. USA
Vol. 90, pp. 7819–7823, August 1993
Neurobiology

N-Methyl-D-aspartate receptors are clustered and immobilized on dendrites of living cortical neurons

TIMOTHY A. BENKE*, OWEN T. JONES†, GRAHAM L. COLLINGRIDGE‡, AND KIMON J. ANGELIDES*§

Departments of §Cell Biology and *Neuroscience, Baylor College of Medicine, Houston, TX 77030; †Playfair Neuroscience Unit, Toronto Western Hospital, Toronto, ON, Canada M5T 2S8; and ‡Department of Pharmacology, University of Birmingham, Birmingham B15 2TT United Kingdom

Communicated by Gordon G. Hammes, April 26, 1993

ABSTRACT **The response of nerve cells to synaptic inputs and the propagation of this activation is critically dependent on the cell-surface distribution of ion channels. In the hippocampus, Ca^{2+} influx through *N*-methyl-D-aspartate receptors (NMDAR) and/or voltage-dependent calcium channels on dendrites is thought to be critically involved in long-term potentiation, neurite outgrowth, epileptogenesis, synaptogenesis, and cell death. We report that conantokin-G (CntxG), a peptide from *Conus geographus* venom, competitively blocked with high affinity and specificity NMDAR-mediated currents in hippocampal neurons and is a reliable probe for exploring NMDAR distribution. Fluorescent derivatives of CntxG were prepared and used to directly determine NMDAR distribution on living hippocampal neurons by digital imaging and confocal fluorescence microscopy. In hippocampal slices, the CA1 dendritic subfield was strongly labeled by CntxG, whereas the CA3 mossy fiber region was not. On CA1 hippocampal neurons in culture, dendritic CntkG-sensitive NMDAR were clustered at sites of synaptic contacts, whereas somatic NMDAR were distributed diffusely and in patches. NMDAR distribution differed from the distribution of voltage-dependent calcium channels. A significant fraction of labeled NMDAR on somata and dendrites was found to be highly mobile: rates were consistent with the possible rapid recruitment of NMDAR to specific synaptic locations. The localization of NMDAR and modulation of this distribution demonstrated here may have important implications for the events that underlie neuronal processing and synaptic remodeling during associative synaptic modification.**

The *N*-methyl-D-aspartate (NMDA)-type of glutamate receptor (NMDAR) (1) plays a specific role in neuronal signaling because activation leads to Ca^{2+} influx (2, 3). Recent studies suggest that synaptic activation of NMDAR leads to focal accumulations of calcium in dendrites and spines (4). Ca^{2+} influx through NMDAR, which has been related to the distribution of NMDAR, may mediate Ca^{2+}-activated processes involved in long-term potentiation (5–7), neurite outgrowth (8), epileptogenesis (9), synaptogenesis (10), and cell death (11). Autoradiography (12) has identified cell populations with NMDA-displaceable glutamate-binding sites, whereas a low-resolution picture of NMDAR on dendrites has emerged from electrophysiological measurements (13–15).

Conantokin-G (CntxG), an unusual peptide from *Conus* venom (16–19), has been reported to be a competitive antagonist of NMDA-induced currents in *Xenopus* oocytes injected with whole-brain mRNA (20). We have shown by electrophysiology that CntxG is a competitive, high-affinity NMDAR-specific ligand on neurons that express native NMDAR, and we have prepared biologically active derivatives of CntxG to determine the distribution and mobility of NMDAR on living neurons by fluorescence microscopy.

The publication costs of this article were defrayed in part by page charge payment. This article must therefore be hereby marked "*advertisement*" in accordance with 18 U.S.C. §1734 solely to indicate this fact.

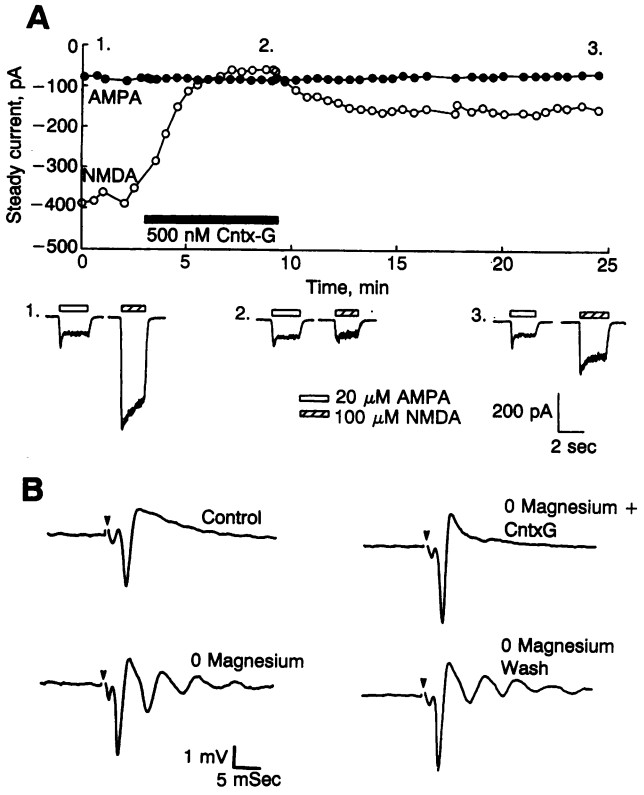

FIG. 1. Inhibition of NMDA-evoked currents in CA1 hippocampal neurons by CntxG. (*A*) Time course of CntxG inhibition. Steady current evoked by applications (marked by bars) of NMDA (100 μM) or AMPA (20 μM) was plotted versus time. Application of CntxG (500 nM), denoted by the bar, reduced NMDA-induced currents 91 ± 3% with a τ_{block} of 2.5 ± 0.6 min (SE, n = 7). On average, NMDA-induced currents remained blocked (61 ± 7%, SE, n = 4) after 15 min of wash-out. AMPA-induced currents were unaffected throughout the experiment. NMDA- and AMPA-induced currents before CntxG application (*1*), during CntxG application (*2*), and after CntxG wash-out (*3*) are shown at bottom. (*B*) Secondary population spikes, recorded from the CA1 stratum pyramidale region of hippocampal slices, which are unmasked by the wash-out of Mg^{2+}, are blocked by CntxG (1 μM). Discontinuities and arrowheads denote blanking of stimulus artifacts.

METHODS

Electrophysiology. Rat hippocampal cultures were prepared as described (21). Recordings of membrane current using tight-seal, whole-cell voltage clamping at 25°C began 4 min after whole-cell rupture. The extracellular solution (ES)

Abbreviations: NMDA, *N*-methyl-D-aspartate; CntxG, conantokin-G; NMDAR, NMDA receptor(s); VDCC, voltage-dependent calcium channels; TmRhd, tetramethylrhodamine; CapBi, caproylbiotin; APV, 2-amino-5-phosphonopentanoic acid; AMPA, α-amino-3-hydroxy-5-methyl-4-isoxazole propionate.

§To whom reprint requests should be addressed.

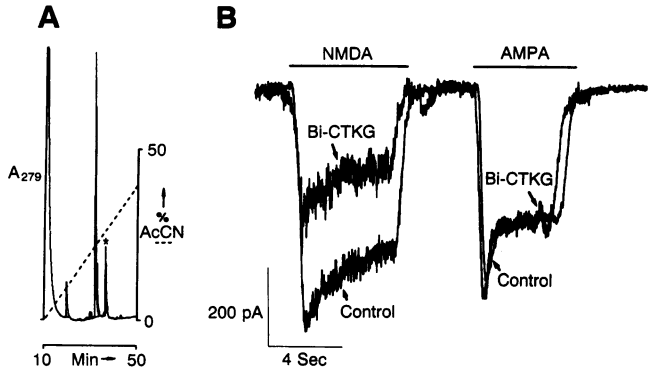

FIG. 2. Purification and characterization of CapBi-CntxG analog. (*A*) HPLC chromatogram of purification of CapBi-CntxG (*) from reaction intermediates. (*B*) CapBi-CntxG (Bi-CTKG; 500 nM) reduced the NMDA (40 μM)-induced current 68% (application marked by bar) to -154 ± 14 pA (SE, $n = 3$). The average induced current responses to NMDA (40 μM) of cells not treated with derivative was -480 ± 35 (SE, $n = 6$) pA. Non-NMDA (AMPA, 20 μM)-induced currents (application marked by bar) were not affected. Due to small amounts of CapBi-CntxG available, neurons were incubated in the derivative for at least 10 min before application of agonists. These currents were compared to control agonist currents in which neurons were not incubated in the derivative.

contained 150 mM NaCl, 3 mM KCl, 10 mM Hepes, 10 mM D-glucose, 2 mM $CaCl_2$, 0.01 mM glycine (pH 7.35). Pipette solutions contained 130 mM CsOH or KOH, 20 mM CsCl or KCl, 10 mM EGTA, 10 mM Hepes, 5 mM NaCl, 140 mM $HMeSO_3$ (pH 7.35). Drugs were applied through multiple-barrel sewer pipes. The holding potential was -60 mV. Transverse hippocampal slices from 5-week-old female rats were perfused with oxygenated solution at 32°C containing 124 mM NaCl, 26 mM $NaHCO_3$, 3 mM KCl, 1.25 mM NaH_2PO_4, 2 mM $CaCl_2$, 2 mM $MgSO_4$, 10 mM D-glucose. Extracellular recordings were made with a 3 mM NaCl-filled glass microelectrode placed in the stratum pyramidale. Responses were elicited in the stratum radiatum every 30 sec.

Preparation of Modified CntxG. CntxG was prepared by solid-phase synthesis (17). Tetramethylrhodamine (TmRhd), Bodipy, and caproylbiotin (CapBi) analogs of CntxG were prepared by acylation with their succinimidyl esters (Molecular Probes) at 1:1 molar ratios (CntxG/ester) in bicarbonate buffer at pH 9.5 at 25°C for 2–6 hr. The monomodified derivatives were purified by reverse-phase HPLC on a Vydac C_{18} column using a linear gradient of 0%–100% CH_3CN in 0.1% trifluoroacetic acid, characterized by hybrid tandem MS,¶ and tested for their ability to block NMDA-induced currents in hippocampal neurons as described above.

Confocal Fluorescence Microscopy. Transverse hippocampal slices (200–300 μm) from 14-day-old female rats were incubated with 50 to 250 nM Bodipy-CntxG in ES at 4°C for 30–60 min followed by three washes with ES (1 min each) and imaged through a ×10, 0.25-numerical aperature objective by scanning laser confocal microscopy (Bio-Rad model 500) 9–30 min after the final wash with ES. Nonspecific labeling was measured on the same field by displacing Bodipy-CntxG with unlabeled CntxG (1 μM) for 1 hr at 25°C.

Digital Epifluorescence Microscopy. CA1 hippocampal cells 10 days in culture were washed three times with ES, incubated with 100–250 nM TmRhd-CntxG for 1 hr at 4°C and washed with ES; sequential differential interference contrast and fluorescence images of living neurons were obtained through a ×63, 1.4-numerical aperature oil-immersion objective using a cooled charge-coupled device camera. Cells were washed in ES, fixed with cold (−20°C) methanol, air-dried, rinsed with 10% goat serum/phosphate-buffered saline (GS-PBS), and incubated with rabbit polyclonal antibodies to

¶Orkiszewski, R. S., Jones, O. T., Angelides, K. J. & Gaskell, S. J., Proceedings of the 39th ASMS Conference on Mass Spectroscopy and Applied Topics, May 19–24, 1991, Nashville, TN.

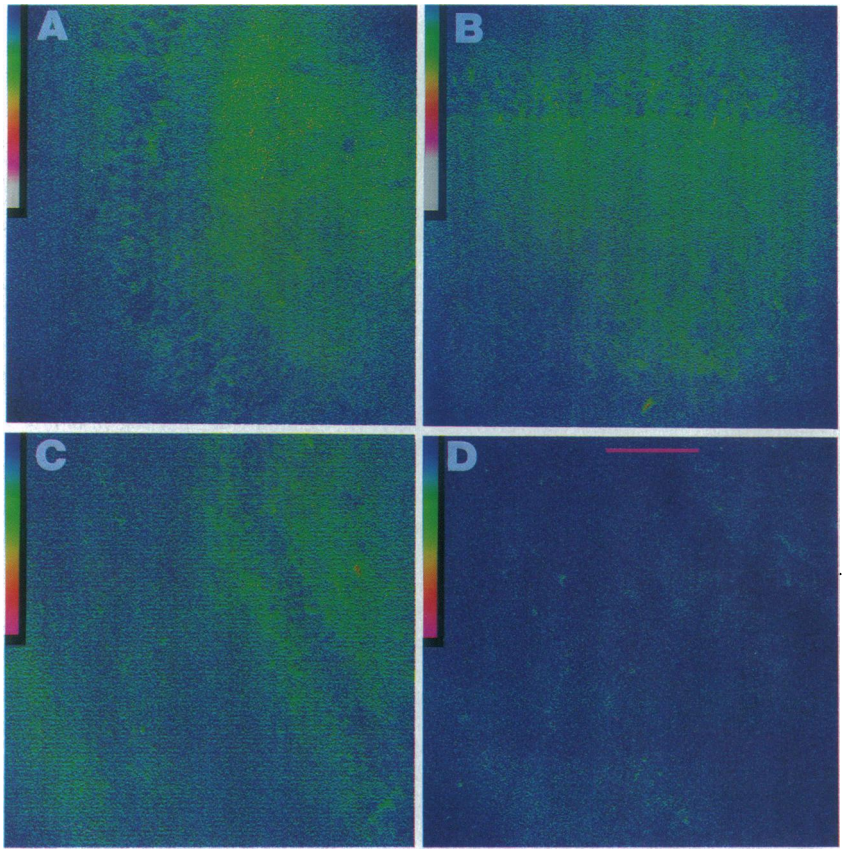

FIG. 3. Distribution of NMDAR in hippocampal slices using Bodipy-CntxG. (*A*) In the CA3 region the light fluorescently outlined cell-body region forms a "(" shape at left. The mossy fiber region inside this "(" shape is less fluorescently labeled, whereas the distal stratum radiatum region is intensely labeled (bright colors). (*B*) In the CA1 region the light fluorescently outlined cell-body layer stretches across the top. The stratum radiatum beneath this region is intensely labeled. (*C*) In the dentate gyrus, the light fluorescently outlined cell-body layer stretches in a "\" shape across the right-hand side. Left of this "\" shape are the intensely fluorescent inputs to the dentate gyrus from the entorhinal cortex; right of the "\" shape is the fluorescent region of dentate gyrus hilar interneurons and then the unfluorescent mossy fiber region. The same slice in *C* is shown in *D* 1 hr after displacement of Bodipy-CntxG by native CntxG. (Bar = 100 μm.)

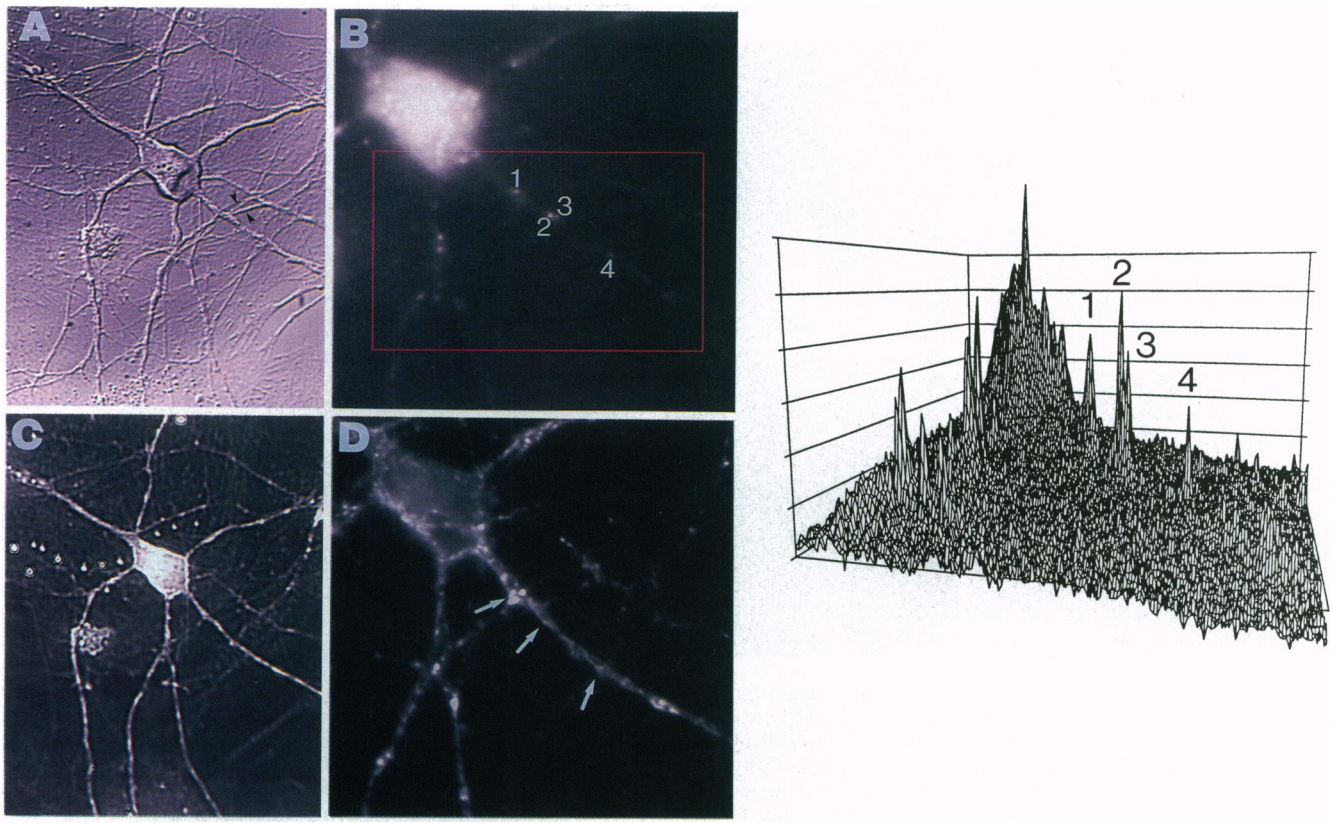

FIG. 4. Distribution of NMDAR on cultured CA1 hippocampal neurons. (*A*) Differential epifluorescence contrast image outlines the neuron and processes from other neurons, the underlying substratum, and putative axonal processes (black arrowheads). (*B*) Distribution of NMDAR on this neuron after incubation in TmRhd-CntxG and digital epifluorescence imaging. Images in *B* and *D* are digitally enlarged by ×2 compared with *A* and *C* for detail. The fluorescent intensity values for each pixel in the red square (58 μm × 35 μm) were topographically mapped at right. Fluorescence intensity is on the vertical axis. Peaks associated with fluorescent patches are numbered at right and correspond to those numbered on the image; fluorescence associated with the cell body is in the left-rear portion. Dendritic clusters were seen at 10 μm (peak 1), 18 μm (peaks 2 and 3), and 31 μm (peak 4) from the cell body. Individual clusters, which were as small as 1.4 μm^2, showed similar peak intensity levels to the soma. (*C*) Dendrites were identified after fixation and labeling with antibodies to microtubule-associated protein 2 (26). (*D*) Synaptic regions, outlined by labeling with antibodies to synaptophysin (27), correspond to patches of NMDAR (arrows correspond to synaptic regions associated with patches numbered in *B* and at right).

microtubule-associated protein 2 (1:100) and mouse monoclonal antibodies to synaptophysin (Boehringer, 1:20). Cells were washed with GS-PBS, incubated with rhodamine-labeled goat antibody to rabbit IgG and fluorescein-labeled goat antibody to mouse IgG, washed with GS-PBS, and reimaged. The distribution of NMDAR and voltage-dependent calcium channels (VDCC) were visualized on the same neuron by labeling with CapBi-CntxG and CapBi-ω-conotoxin linked to fluorescent green and red latex beads, respectively.

Fluorescence Photobleach Recovery. Visual cortex neurons 14 days in culture were labeled with 250 nM TmRhd-CntxG in ES for 1 hr at 4°C and washed with ES at 25°C. The diffusion coefficient (D_L) and mobile fraction (f) of fluorescently labeled CntxG-sensitive NMDA receptors at room temperature were obtained by the spot photobleaching technique (22) and curve-fitting procedures (23). Incomplete fluorescence recovery was attributed to immobility of a fraction of the fluorophores on the time scale of the experiment. Dendritic regions where D_L and f were measured were usually ≈2 μm in diameter and thus were greater than or equal to the diameter of the laser beam; D_L and f could be underestimated by ≈15% in smaller regions (24).

RESULTS

CntxG Blocks NMDAR-Mediated Neuronal Currents. CntxG substantially reduced the inward current induced by NMDA in cultured hippocampal neurons (Fig. 1*A*). The effect developed over 5 min but reversed slowly and incompletely. The NMDA-induced response remained blocked after 45 min of washing (data not shown), demonstrating high affinity. Coapplication of CntxG with D(−)-2-amino-5-phosphonopentanoic acid (D-APV, Tocris Neuramin, Bristol, U.K.), a known competitive antagonist of NMDAR (1), prevented the sustained block of NMDA-induced responses (see Fig. 5*B*) observed in the same neuron by application of CntxG alone. CntxG was specific: it had no effect on the inward current evoked by α-amino-3-hydroxy-5-methyl-4-isoxazole propionate (AMPA, Tocris Neuramin), a non-NMDA glutamate-receptor agonist (1) (Fig. 1*A*), sodium currents, potassium currents, or VDCC currents (data not shown). CntxG had access to and selectively blocked the NMDAR-mediated component of hippocampal synaptic transmission (Fig. 1*B*).

Chemical Modification and Characterization of Modified CntxG. Separation of native CntxG from starting materials and mono- and bi-modified CntxG by HPLC is shown in Fig. 2*A*. Modification did not adversely affect the biological activity of CntxG. CapBi-CntxG reduced whole-cell NMDA-induced currents in patch-clamped hippocampal neurons (Fig. 2*B*) and also in cerebellar granule cells (72%, $n = 5$) with little reversibility after 10 min of wash-out.

Distribution of NMDAR on Living Neurons. We used fluorescent CntxG to determine more directly the distribution of functional CntxG-sensitive NMDAR in living slices. The resulting pattern (Fig. 3) was characteristic of NMDAR

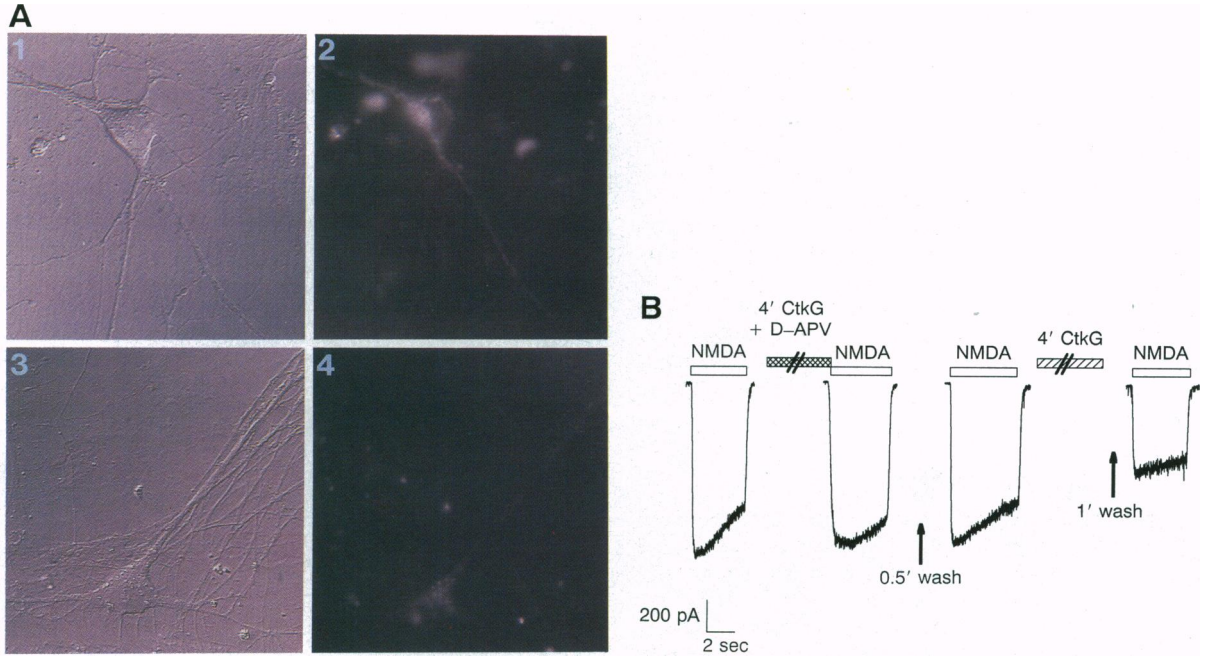

FIG. 5. D-APV, a competitive NMDAR antagonist, prevents binding of CntxG to NMDAR. (*A*) Two neurons with processes and substrata in *1* and *3*. The neuron in *1* was incubated with 100 nM TmRhd-CntxG for 1 hr at 4°C. The neuron in *3* was incubated with 100 nM TmRhd-CntxG plus 1 mM D-APV for 1 hr at 4°C. The labeling of NMDAR on the neuron in *4* (3087 ± 136, mean ± SE integrated somatic and dendritic fluorescence intensity, $n = 2$ neurons) is seen to be substantially less than that on the neuron in *2* (4640 ± 496, mean ± SE integrated somatic and dendritic fluorescence intensity, $n = 5$ neurons) on both dendrites and somata. Integrated nonspecific fluorescence measured on neurons labeled with 100 nM TmRhd-CntxG plus 100 μM native CntxG for 1 hr at 4°C was 3044 ± 349 (mean ± SE, $n = 3$ neurons). (*B*) Control NMDA (40 mM, application indicated by clear bars)-induced currents in a cultured hippocampal neuron are not significantly affected by a 4-min coapplication of 500 nM CntxG (CtkG) and 100 μM D-APV (application indicated by cross-hatched bar). The time course of NMDA-induced currents immediately after removal of D-APV and CntxG is initially altered but recovers to control after 0.5-min wash. Application of 500 nM CntxG alone (indicated by hatched bar) to the same neuron for 4 min significantly blocked NMDA-induced currents, similar to Fig. 1*A*.

subfields in the hippocampus (12), providing further evidence for the selectivity of CntxG for NMDAR.

To show whether or not NMDAR are localized at synapses (14), as well as at extrasynaptic sites (25), we labeled CA1 hippocampal neurons in culture with TmRhd-CntxG (Fig. 4). Digital fluorescence imaging showed that CntxG-sensitive NMDAR were heterogeneously distributed and localized to soma and processes (Fig. 4*B*), as outlined by a differential interference contrast image of the neuron (Fig. 4*A*). Somatic fluorescence was interspersed with patches of intense fluorescence, whereas dendrites (Fig. 4*C*) had only patches of intense fluorescence. Each dendritic NMDAR cluster was associated with a synaptic contact on the neuron (Fig. 4*D*). These experiments confirm the specificity of CntxG labeling. Fibroblasts and glial cells, cells that do not express NMDAR and form part of the underlying substratum in these cultures, were not labeled, although they do express other receptors and channels, including non-NMDA glutamate receptors on their surface (28). Also, neurons incubated with TmRhd-CntxG and D-APV showed substantially reduced labeling (Fig. 5*A*, *3* and *4*), compared with neurons labeled under identical optical conditions with TmRhd-CntxG alone (Fig. 4 *A* and *B* and Fig. 5*A*, *1* and *2*).

Because Ca^{2+} entry into neurons through both NMDAR and/or VDCC may initiate the biochemical processes that underlie such processes as long-term potentiation (7), we examined the spatial relationship of these two types of channels. Double-labeled neurons (Fig. 6 *A* and *B*) showed

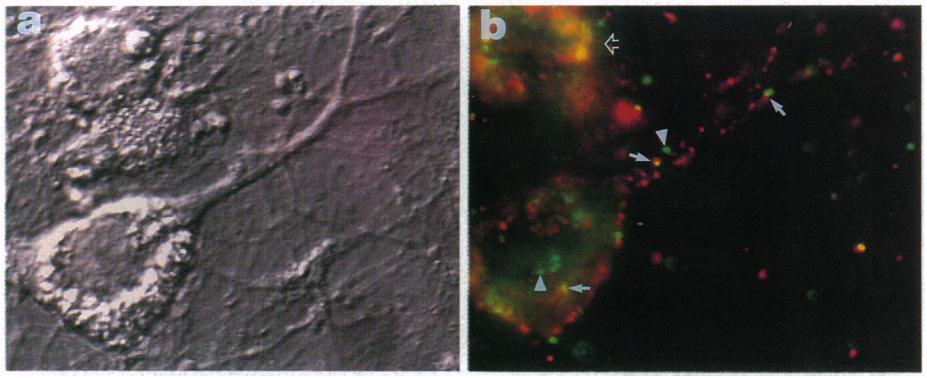

FIG. 6. Comparison of the distribution of VDCCs and NMDAR on an individual neuron. (*A*) Differential interference contrast image of a neuron with processes, substrata, and a neighboring neural soma (outlined arrowhead). (*B*) Overlay of two digital epifluorescent images shows ω-conotoxin-sensitive VDCC in red and CntxG-sensitive NMDAR in green. Yellow overlapping regions along a microtubule-associated protein 2-positive dendrite are denoted by arrows. These images show that the two populations of receptors are sometimes in the same location and sometimes not in the same location (arrowhead), with regard to both somata and dendrites.

that VDCC and NMDAR have distinct distributions on somata and dendrites. VDCC are more widely distributed along dendrites and dendritic shafts compared with NMDAR. However, at least at the level of the light microscope, some receptor clusters had overlapping distributions.

Fluorescence Photobleach Recovery. We measured the lateral mobility of TmRhd-CntxG-labeled NMDAR by fluorescence photobleach recovery to determine whether the heterogeneous distribution of NMDAR is maintained partly by receptor restriction. Fluorescence photobleach recovery showed that 73 ± 4.7% (mean ± SD, $n = 9$) of the receptors on the cell body and dendrites were immobile, with diffusion coefficients $\leq 1 \times 10^{-12}$ cm^2/sec. However, 27% of the receptors moved at rates of $7.0 \pm 3.5 \times 10^{-10}$ cm^2/sec (mean ± SD, $n = 9$), which is at the upper limit for membrane protein diffusion (29).

DISCUSSION

CntxG and derivatives selectively and competitively blocked with high affinity and specificity NMDA-induced currents in hippocampal pyramidal and cerebellar granule neurons. These results support reports that CntxG is a competitive antagonist of NMDA-induced currents in *Xenopus* oocytes injected with mouse-brain mRNA (20). However, in this expression system it is unknown which NMDA-subunit subtypes are expressed and whether or not they are assembled in the same subunit composition as *in vivo*. Even at very high concentrations of CntxG, the block remained incomplete (Fig. 1*A*), suggesting the possibility that CntxG may be a selective antagonist for a subpopulation of NMDAR in these neurons. Indeed, at least two of the four known NMDAR-subunit subtypes have been localized by *in situ* hybridization histochemistry in the hippocampus (30).

The specificity of CntxG binding to NMDAR was demonstrated by electrophysiology and by imaging experiments that showed that only neurons were labeled and not the underlying substrata. Because D-APV competes with CntxG for neuronal labeling and current blockade, CntxG is likely to bind to NMDAR near the agonist-binding site.

The functional role of NMDAR clusters on somata, reported consistently in single-channel studies (31) and demonstrated here, is not known. The highly punctate distribution of the CntxG-sensitive population of NMDAR on dendrites has several implications for mediating Ca^{2+} entry and neuronal processing. The patchy distribution of NMDAR at sites of synaptic contact on hippocampal dendrites differs strikingly from the more extensive distribution of N-type VDCC throughout the dendrites (32) or L-type VDCC at the base of apical dendrites (33). The highly punctate distribution of NMDAR had dimensions suggestive of dendritic spines; their localization in these synaptic regions would be consistent with models (34) in which focal calcium accumulation and sequestration (4, 35) activate local biochemical mechanisms (36).

Although the forces that limit the mobility of NMDAR are likely to contribute to their regional localization, the presence of a pool of rapidly mobile receptors hints at another mechanism for NMDAR dynamics. From the relationship $r^2 = 4D_L t$, where r is the average distance, D_L is the diffusion coefficient, and t is time, ≈25% of NMDAR could move across an average spine head (34) (0.6 μm^2) in ≈2 sec. The rapid movement of NMDAR to sites of high synaptic activity could further enhance the local Ca^{2+} concentration underneath the membrane. The recruitment and redistribution of the mobile fraction of NMDAR in response to synaptic activity is a possibility: theoretical calculations suggest that synaptic activity can induce receptor clustering (37), and the NMDAR-mediated component of synaptic responses has been shown to undergo long-term potentiation (38). It is possible that NMDAR activation and resulting Ca^{2+} influx can activate Ca^{2+}-mediated proteolysis of fodrin (39), increasing NMDAR mobility by releasing it from lateral constraints.

We thank R. U. Rodriguez, M. Zarei, and A. J. Irving for cell cultures and John Dani and K.J.A.'s laboratory group for very helpful discussions. Antibodies to microtubule-associated protein 2 were a generous gift from R. Vallee. This work was supported by grants from the National Institutes of Health to K.J.A., a Research Fellowship from the American Epilepsy Foundation to O.T.J., Medical Scientist Training Program and Achievement Rewards for College Scientists awards to T.A.B., a Wellcome Trust grant to G.L.C., and a Human Frontiers of Science Award to K.J.A. and G.L.C.

1. Collingridge, G. L. & Lester, R. A. J. (1989) *Pharmacol. Rev.* **41**, 143–210.
2. Ascher, P. & Nowak, L. (1988) *J. Physiol. (London)* **399**, 247–266.
3. Mayer, M. L. & Westbrook, G. L. (1987) *J. Physiol. (London)* **394**, 501–527.
4. Muller, W. & Connor, J. A. (1991) *Nature (London)* **354**, 73–76.
5. Collingridge, G. L., Kehl, S. J. & McLennan, H. (1983) *J. Physiol. (London)* **334**, 33–46.
6. Lynch, G., Larson, J., Kelso, S., Barrionuevo, G. & Schottler, F. (1983) *Nature (London)* **305**, 719–721.
7. Malenka, R. C., Kauer, J. A., Zucker, R. S. & Nicoll, R. A. (1988) *Science* **242**, 81–84.
8. Mattson, M. P., Dou, P. & Kater, S. B. (1988) *J. Neurosci.* **8**, 2087–2100.
9. Croucher, M. J., Collins, J. F. & Meldrum, B. S. (1982) *Science* **21**, 899–901.
10. Rabacchi, S., Bailly, Y., Delhaye-Bouchaud, N. & Mariani, J. (1992) *Science* **256**, 1823–1825.
11. Choi, D. W. (1988) *Trends Neurosci.* **11**, 465–469.
12. Monaghan, D. T., Holets, V. R., Toy, D. W. & Cotman, C. W. (1983) *Nature (London)* **306**, 176–179.
13. Arancio, O. & MacDermott, A. B. (1991) *J. Neurophysiol.* **65**, 899–913.
14. Bekkers, J. M. & Stevens, C. F. (1989) *Nature (London)* **341**, 230–233.
15. Jones, K. A. & Baughman, R. W. (1991) *Neuron* **7**, 593–603.
16. Olivera, B. M., Gray, W. R., Zeikus, R., McIntosh, J. M., Varga, J., Rivier, J., de Santos, V. & Cruz, L. J. (1985) *Science* **230**, 1338–1343.
17. Rivier, J., Galyean, R., Simon, L., Cruz, L. J., Olivera, B. M. & Gray, W. R. (1987) *Biochemistry* **26**, 8508–8512.
18. Olivera, B. M., McIntosh, J. M., Clark, C., Middlemas, D., Gray, W. R. & Cruz, L. J. (1985) *Toxicon* **23**, 277–282.
19. Mena, E. E., Gullak, M. F., Pagnozzi, M. J., Richter, K. E., Rivier, J., Cruz, L. J. & Olivera, B. M. (1990) *Neurosci. Lett.* **118**, 241–244.
20. Hammerland, L. G., Olivera, B. M. & Yoshikami, D. (1992) *Eur. J. Pharmacol.* **226**, 239–244.
21. Banker, G. A. & Cowan, W. M. (1977) *Brain Res.* **126**, 397–425.
22. Koppel, D. E. (1979) *Biophys. J.* **28**, 281–292.
23. Axelrod, D., Koppel, D. E., Schlessinger, J., Elson, E. & Webb, W. W. (1976) *Biophys. J.* **16**, 1055–1069.
24. Angelides, K. J., Elmer, L. W., Loftus, D. & Elson, E. (1989) *J. Cell Biol.* **106**, 1911–1925.
25. Dingledine, R. (1986) *Trends Neurosci.* **9**, 47–49.
26. Caceres, A., Banker, G. A. & Binder, L. (1986) *J. Neurosci.* **6**, 714–722.
27. Johnston, P. A., Jahn, R. & Sudhof, T. C. (1989) *J. Biol. Chem.* **264**, 1268–1273.
28. Blankenfeld, G. V. & Kettenmann, H. (1991) *Mol. Neurobiol.* **5**, 31–43.
29. Cherry, R. J. (1979) *Biochim. Biophys. Acta* **559**, 289–327.
30. Monyer, H., Sprengel, R., Schoepfer, R., Herb, A., Higuchi, M., Lomeli, N., Burnashev, N., Sakmann, B. & Seeburg, P. H. (1992) *Science* **256**, 1217–1221.
31. Cull-Candy, S. G. & Usowicz, M. M. (1987) *Nature (London)* **325**, 525–528.
32. Jones, O. T., Kunze, D. L. & Angelides, K. J. (1989) *Science* **244**, 1189–1193.
33. Westenbroek, R. E., Ahlijanian, M. K. & Catterall, W. A. (1990) *Nature (London)* **347**, 281–284.
34. Harris, K. M. & Stevens, J. K. (1989) *J. Neurosci.* **9**, 2982–2997.
35. Guthrie, P. B., Segal, M. & Kater, S. B. (1991) *Nature (London)* **354**, 76–80.
36. Hannun, Y. A., Loomis, C. R. & Bell, R. M. (1986) *J. Biol. Chem.* **261**, 7184–7190.
37. Fromherz, P. (1988) *Proc. Natl. Acad. Sci. USA* **85**, 6353–6357.
38. Bashir, Z. I., Alford, S., Davies, S. N., Randall, A. D. & Collingridge, G. L. (1991) *Nature (London)* **349**, 156–158.
39. Di Stasi, A. M. M., Gallo, V., Ceccarini, M. & Petrucci, T. C. (1991) *Neuron* **6**, 445–454.